Inorg. Chem. **2003**, *42*, 4456–4468

Dinuclear Copper(I) Complexes with Hexaaza Macrocyclic Dinucleating Ligands: Structure and Dynamic Properties

Miquel Costas,[†] Raul Xifra,[†] Antoni Llobet,*[,†] Miquel Solà,*[,†] Juvencio Robles,[†,‡] Teodor Parella,[§] Helen Stoeckli-Evans,[||] and Markus Neuburger[⊥]

Departament de Química, Universitat de Girona, Campus de Montilivi E-17071, Girona, Spain, Departament de Química and Institut de Química Computacional, Universitat de Girona, Facultad de Química, Universidad de Guanajuato, Noria Alta s/n, Guanajuato, GTO, 36050, Mexico, Servei de RMN, Universitat Autònoma de Barcelona, Bellaterra E-08193, Barcelona, Spain, Institute of Chemistry, University of Neuchatel, Av. Bellevaux 51, CH-2000, Neuchatel, Switzerland, and Institut für Anorganische Chemie der Universität Basel Spitalstrasse 51, 4056 Basel, Switzerland

Received November 16, 2002

The synthesis and structural and spectroscopic characterization of a family of copper(I) complexes, containing a dinucleating hexaaza macrocyclic ligand, of general formula $[Cu_2(L)(X)_2]^{2+}$ (L = Me2p, Me2m, Me3p, or Me3m; X = MeCN, *n*-PrCN, CO, *t*-BuNC, or PPh_3) is described. This family of complexes contains ligands that differ from one another in the number of methylenic units linking the tertiary amines and in the meta or para substitution of their aromatic rings. The structural characterization in the solid-state includes a single-crystal X-ray diffraction analysis of $[Cu_2(Me2p)(CO)_2]^{2+}$ and of $[Cu_2(Me2m)(t\text{-}BuNC)_2]^{2+}$. In solution, those complexes are structurally characterized through NMR spectroscopy that also allows us to put forward and establish their fluxional behavior. Theoretical calculations at the DFT level have also been performed in order to further analyze the relative energy of the different potential isomers as well as to gain insight into their chemical properties. Finally, the influence of the hexaaza ligands over different structural aspects as well as on its potential chemical reactivity is discussed.

Introduction

Nature has taken advantage of cooperation phenomena between metal centers in the design of several metalloproteins where the close proximity of two metal centers mediates reactions that range from small molecule activation (N_2, O_2, H_2)[1−4] to hydrolysis.[5] Proteins containing dinuclear copper centers are involved in a number of biologically important processes that extend from electron transfer to O_2 transport or activation.[6−10] For example, hemocyanin, the O_2 carrier protein in arthropods and mollusks, contains a dinuclear copper center in its active site. In the oxy and deoxy forms, each of the copper atoms is bound to three histidine residues.[11] Tyrosinase has a very similar active site, but its biological role is the ortho hydroxylation of phenols to catechols and catechols to quinones.[4,12] Catechol oxidases also contain nitrogen rich dinuclear copper centers in their active site and mediate the oxidation of catechols to

* To whom correspondence should be addressed. E-mail: antoni.llobet@udg.es.

[†] Departament de Química and Institut de Química Computacional, Universitat de Girona.

[‡] Permanent address: Facultad de Química, Universidad de Guanajuato, Noria Alta s/n, Guanajuato, GTO, 36050, Mexico.

[§] Servei de RMN, Universitat Autònoma de Barcelona, Bellaterra E-08193, Barcelona, Spain.

[||] Institute of Chemistry, University of Neuchatel, Av. Bellevaux 51, CH-2000, Neuchatel, Switzerland.

[⊥] Institut für Anorganische Chemie der Universität Basel Spitalstrasse 51, 4056 Basel, Switzerland.

(1) Howard, J. B.; Rees, D. C. *Chem. Rev.* **1996**, *96*, 2965−2982.
(2) Wallar, B. J.; Lipscomb, J. D. *Chem. Rev.* **1996**, *96*, 2625−2658.
(3) Thauer, R. K.; Klein, A. R.; Hartmann, G. C. *Chem. Rev.* **1996**, *96*, 3031−3042.
(4) Solomon, E. I.; Chen, P.; Metz, M.; Lee, S.-K.; Palmer, A. E. *Angew. Chem.* **2001**, *113*, 4702−4724; *Angew. Chem., Int. Ed.* **2001**, *40*, 4570−4590.
(5) Wilcox, D. E. *Chem. Rev.* **1996**, *96*, 2435−2458.
(6) *Bioinorganic Chemistry of Copper*; Karlin, K. D., Tyeklár, Z., Eds.; Chapman & Hall: New York, 1993.
(7) Kitajima, N.; Moro-oka, Y. *Chem. Rev.* **1994**, *94*, 737−757.
(8) Karlin, K. D.; Fox, S. In *Active Oxygen in Biochemistry, Vol. 3*; Valentine, J. S., Foote, C. S., Greenberg, A., Liebman, J. F., Eds.; Chapman & Hall: Glasgow, 1995; pp 188−231.
(9) Klinman, J. P. *Chem. Rev.* **1996**, *96*, 2541−2561.
(10) Robb D. A. In *Copper Proteins and Copper Enzymes, Vol 2*; Lontie, R., Ed.; CRC: Boca Raton, FL, 1984.
(11) Magnus, K. A.; Ton-That, H. J.; Carpenter, E. *Chem. Rev.* **1994**, *94*, 727−735.
(12) Solomon, E. I.; Sundaram, U. M.; Machonkin, T. E. *Chem. Rev.* **1996**, *96*, 2563−2605.

10.1021/ic0261833 CCC: $25.00
Published on Web 06/07/2003

quinones.[13] The activity of all these metalloproteins relies on the cooperative activity of the two copper centers, and therefore, the relative spatial arrangement of the two metal centers is a key issue. For example, dioxygen binding in hemocyanin or tyrosinase results in the formation of peroxo−Cu_2 species,[12] and the enzymatic activity of catechol oxidases has been attributed to the simultaneous binding of the catechol to the two copper centers.[13] Structural and functional modeling of these enzymes has been a subject of great interest in bioinorganic chemistry. In fact, model compounds have played a key role in the understanding of the spectroscopic and structural properties of oxyhemocyanin and oxytyrosinase,[4,12] and indeed, some of these models have reproduced the main spectroscopic and structural features of the natural systems.[14−16] Modeling of the nitrogen rich active site of these enzymes has been achieved by using ligand architectures based on aromatic amines or Schiff bases.[17,18] In this context, the ability of macrocyclic ligands to preorganize two metal centers with a particular Cu···Cu distance has been used in the design of dinuclear Cu complexes with Schiff base macrocyclic ligands as structural and functional models of dinuclear copper monooxygenases and copper oxidases.[19−26] Recent work has also been focused on using copper(I) complexes containing aliphatic amine ligands as functional models, and a reversible O−O bond breaking and forming system has been described using these types of ligands.[27−29] With few exceptions though,[30,31] the studies have been limited to mononuclear complexes where the relative spatial arrangement cannot be controlled.[17,18]

In this work, we are presenting the synthesis and spectroscopic and structural characterization of a series of dinuclear copper(I) complexes containing hexaaza macrocyclic ligands that solely contain tertiary amines. These macrocyclic ligands have been designed to allow the control of electronic, geometric, and spatial properties including the local and the relative Cu metal geometries.

Experimental Section

Caution! Perchlorate salts are all potentially explosive and should be handled with care.

Materials and Synthesis. Solvents were purchased from SDS as reagent grade. Acetonitrile was distilled over P_2O_5 and stored over molecular sieves. Diethyl ether and THF were distilled over Na/benzophenone under nitrogen. CH_2Cl_2 was distilled over CaH_2 and stored over molecular sieves. Methanol was distilled over Mg and stored in the dark over molecular sieves. Acetone was dried over $CaCl_2$ and stored over molecular sieves. Butyronitrile was used as received. Unless noted otherwise, all reagents were purchased from commercial sources and used as received. Preparation and handling of air-sensitive materials were carried out under argon or N_2 atmosphere using standard Schlenk techniques.

3,6,9,16,19,22-Hexamethyl-3,6,9,16,19,22-hexaazatricyclo-[22.2.2.$2^{11,14}$]triaconta-1(26),11(12),13,24,27,29-hexaene, Me2p, 3,6,9,-17,20,23-hexamethyl-3,6,9,17,20,23-hexaazatricyclo[23.3.1.$1^{11,15}$]-triaconta-1(29),11(30),12,14,25,27-hexaene, Me2m, 3,7,11,18,22,26-hexamethyl-3,7,11,18,22,26-hexaazatricyclo[26.2.2.$2^{13,16}$]tetratriaconta-1(31),13(33),14,16(34),28(32),29-hexaene, Me3p, and 3,7,11,19,23,27-hexamethyl-3,7,11,19,23,27-hexaazatricyclo[27.3.1.$1^{13,17}$]tetratriaconta-1(32),13,15,17(34),29(33),30-hexaene, Me3m, were prepared according to the published procedures or slight modifications thereof.[32−35] [$Cu(CH_3CN)_4$]X, X = ClO_4, PF_6, and CF_3SO_3, were prepared according to the published procedures or slight modifications thereof.[36,37]

[Cu_2(Me2p)(CH_3CN)$_2$](ClO_4)$_2$ (1). Solid Me2p (50 mg, 0.101 mmol) and [$Cu(CH_3CN)_4$]ClO_4 (66 mg, 0.202 mmol) were dissolved in CH_2Cl_2 (3 mL), and the mixture was stirred for 15 min. The solvent was removed under vacuum and the residue recrystallized from CH_3CN/ether 1:3 v/v to obtain a white crystalline solid (75 mg, 0.081 mmol, 81%). FT-IR (KBr): ν = 2260, 1467, 1100 and 625 cm^{-1}. Anal. (%) Calcd for $C_{34}H_{56}N_8Cu_2Cl_2O_8 \cdot H_2O$: C 44.35, N 12.17, H 6.35. Found: C 44.39, N 12.04, H 6.05.^{1}H NMR (CD_3CN, 322 K): δ = 7.60−7.20 (broad, 8H, arom), 4.50−2.00 (broad, 24H, $ArCH_2$ and NCH_2C), 2.65 (s, 18H, NCH_3), 1.99 (s, 6H, CH_3CN).

[Cu_2(Me2p)(*n*-PrCN)$_2$](ClO_4)$_2$ (2). Solid Me2p (50 mg, 0.101 mmol) and [$Cu(CH_3CN)_4$]ClO_4 (66 mg, 0.202 mmol) were dissolved in butyronitrile (1 mL). The solution was vigorously stirred

(13) Gerdemann, C.; Eicken, C.; Krebs, B. *Acc. Chem. Res.* **2002**, *35*, 183−191.
(14) (a) Kitajima, N.; Fujisawa, K.; Moro-oka, Y. *J. Am. Chem. Soc.* **1989**, *111*, 8975−8976. (b) Kitajima, N.; Fujisawa, L.; Fujimoto, C.; Moro-oka, Y.; Hashimoto, S.; Kitagawa, T.; Toriumi, K.; Tatsumi, K.; Nakamura, A. *J. Am. Chem. Soc.* **1992**, *114*, 1277−1291.
(15) (a) Itoh, S.; Kumei, H.; Taki, M.; Nagatomo, S.; Kitagawa, T.; Fukuzumi, S. *J. Am. Chem. Soc.* **2001**, *123*, 6708−6709. (b) Taki, M.; Teramae, S.; Nagatomo, S.; Tachi, Y.; Kitagawa, T.; Itoh, S.; Fukuzumi, S. *J. Am. Chem. Soc.* **2002**, *124*, 6367−6377.
(16) Kodera, M.; Katayama, K.; Tachi, Y.; Kano, K.; Hirota, S.; Fujinami, S.; Suzuki, M. *J. Am. Chem. Soc.* **1999**, *121*, 11006−11007.
(17) Kopf, M.-A.; Karlin, K. D. In *Models for Copper Enzymes and Heme-Copper Oxidases*; Meunier, B., Ed.; Imperial College Press: London, 2000; pp 309−362.
(18) Schindler, S. *Eur. J. Inorg. Chem.* **2000**, 2311−2326.
(19) Menif, R.; Martell, A. E. *J. Chem. Soc., Chem. Commun.* **1989**, *20*, 1521−3.
(20) Rockcliffe, D. A.; Martell, A. E. *J. Chem. Soc., Chem. Commun.* **1992**, 1758−1760.
(21) Rockcliffe, D. A.; Martell, A. E. *Inorg. Chem.* **1993**, *32*, 3143−3152.
(22) Rockcliffe, D. A.; Martell, A. E. *J. Mol. Catal. A: Chem.* **1995**, *99*, 101−114.
(23) Martell, A. E.; Motekaitis, R. J.; Menif, R.; Rockcliffe, D. A.; Llobet, A. *J. Mol. Catal. A: Chem.* **1997**, *117*, 205−213.
(24) Llobet, A.; Martell, A. E.; Martinez, M. A. *J. Mol. Catal. A: Chem.* **1998**, *129*, 19−26.
(25) Utz, D.; Heinemann, F. W.; Hampel, F.; Richens, D. T.; Schindler, S. *Inorg. Chem.* **2003**, *42*, 1430−1436
(26) Ma, H.; Allmendinger, M.; Thewalt, U.; Lentz, A.; Klinga, M.; Rieger, B. *Eur. J. Inorg. Chem.* **2002**, *11*, 2857−2867.
(27) Halfen, J. A.; Mahapatra, S.; Wilkinson, E. C.; Kaderli, S.; Young, V. G., Jr.; Que, L., Jr.; Zuberbühler, A. D.; Tolman, W. B. *Science* **1996**, *271*, 1397−1400.
(28) Mahadevan, V.; Henson, M. J.; Solomon, E. I.; Stack, T. D. P. *J. Am. Chem. Soc.* **2000**, *122*, 10249−10250.
(29) Liang, H.-C.; Zhang, C. X.; Henson, M. J.; Sommer, R. D.; Hatwell, K. R.; Kaderli, S.; Zuberbühler, A. D.; Rheingold, A. L.; Solomon, E. I.; Karlin, K. D. *J. Am. Chem. Soc.* **2002**, *124*, 4170−4171.
(30) Mahapatra, S.; Kaderli, S.; Llobet, A.; Neuhold, Y.-M.; Palanche, T.; Halfen, J. A.; Young, V. G., Jr.; Kaden, T. A.; Que, L., Jr.; Zuberbühler, A. D.; Tolman, W. B. *Inorg. Chem.* **1997**, *36*, 6343−6356.
(31) Mahapatra, S.; Young, V. G., Jr.; Kaderli, S.; Zuberbühler, A. D.; Tolman, W. B. *Angew. Chem.* **1997**, *109*, 125−127; *Angew. Chem., Int. Ed. Engl.* **1997**, *36*, 130−133.
(32) Menif, R.; Martell, A. E.; Squattrito, P. J.; Clearfield, A. *Inorg. Chem.* **1990**, *29*, 4723−4729.
(33) Pietraszkiewicz, M.; Gasiorowski, R. *Chem. Ber.* **1990**, *123*, 405−406.
(34) Llobet, A.; Reibenspies, J.; Martell, A. E. *Inorg. Chem.* **1994**, *33*, 5946−5951.
(35) Clifford, T.; Danby, A. M.; Lightfoot, P.; Richens, D. T.; Hay, R. W. *J. Chem. Soc., Dalton Trans.* **2001**, 240−247.
(36) Kubas, G. J. *Inorg. Synth.* **1990**, *28*, 68−70.
(37) Kubas, G. J. *Inorg. Synth.* **1979**, *19*, 90−92.

for 30 min, and ether (10 mL) was added to precipitate a white solid. The solvent was removed with a syringe and the residue dried under vacuum to obtain a white solid (60 mg, 0.063 mmol, 62%). FT-IR (KBr): ν = 2249, 1467, 1100, and 625 cm^{-1}. Anal. (%) Calcd for $C_{38}H_{64}N_8Cu_2Cl_2O_8 \cdot CH_3CN \cdot 2H_2O$: C 46.37, N 12.17, H 6.91. Found: C 46.37, N 12.23, H 6.73. ^{1}H NMR (CD_3CN, 322 K): δ = 7.45 (s, 8H, arom), 3.74 (s, 8H, $ArCH_2$), 2.85 (s broad, 16H, NCH_2C), 2.69 (s, 6H, NCH_3), 2.37 (t, J = 7 Hz, 4H, CH_2CN), 2.32 (s, 12H, NCH_3), 1.70 (m, 4H, CH_3CH_2 nitrile), 1.09 (t J = 6 Hz, 6H, CH_3 nitrile).

[Cu$_2$(Me2m)(*n*-PrCN)$_2$](PF$_6$)$_2$ (3). [Cu(CH$_3$CN)$_4$]PF$_6$ (87 mg, 0.235 mmol) was dissolved in butyronitrile (3 mL). The solution was stirred for 15 min and the solvent removed under vacuum. The residue was taken in acetone (3 mL). Over this solution was added an acetone (3 mL) solution of Me2m (58 mg, 0.117 mmol), and the mixture was stirred for 10 min. The solvent was removed under vacuum, and the residue was dissolved in butyronitrile/ether 1:5 (v/v) (3 mL) and placed in the fridge. After 24 h, a white microcrystalline product was filtered and dried under vacuum (66 mg, 0.063 mmol, 54%). FT-IR (KBr): ν = 2249, 1472, 841, and 568 cm^{-1}. Anal (%) Calcd for $C_{38}H_{64}N_8Cu_2P_2F_{12}$: C 43.47, N 10.67, H 6.14. Found: C 43.53, N 10.59, H 6.11. ^{1}H NMR (CD_3CN, 298 K): δ = 7.85 (s, 2H, arom), 7.46 (s, 6H, arom.), 3.88 (s, 8H, $ArCH_2$), 2.80 (s broad, 16H, NCH_2C), 2.55 (s, 6H, NCH_3), 2.37 (m, 4H, CH_2CN), 2.32 (s, 12H, NCH_3), 1.70 (m, 4H, CH_3CH_2 nitrile), 1.07 (m, 6H, CH_3 nitrile).

[Cu$_2$(Me3p)](ClO$_4$)$_2$ (4). Me3p (176 mg, 0.320 mmol) was dissolved in CH$_3$OH (15 mL). Over this solution, [Cu(CH$_3$CN)$_4$]ClO$_4$ (209 mg, 0.64 mmol) dissolved in CH$_3$OH (35 mL) was added. The mixture was stirred for 30 min, and the white solid that precipitated was filtered and dried under vacuum (258 mg, 0.288 mmol, 90%). FT-IR (KBr): ν = 1467, 1084, and 620 cm^{-1}. Anal. (%) Calcd for $C_{34}H_{58}N_6Cu_2Cl_2O_8 \cdot H_2O$: C 45.73, N 9.42, H 6.78. Found: C 45.51, N 9.33, H 6.64. ^{1}H NMR (CD_3CN, 298 K): δ = 7.31 (s, 8H, arom), 3.52 (s, 8H, $ArCH_2$), 2.65 (m, 16H, NCH_2), 2.45 (s, 6H, NCH_3), 2.28 (s, 12H, NCH_3), 1.84 (m broad, 8H, $CH_2CH_2CH_2$). ^{13}C NMR (CD_3CN, 298 K): δ = 136.3 (arom ter), 130.1 (arom sec), 62.8 ($ArCH_2$), 59.4 (NCH_2), 43.7, 43.5 (NCH_3), 23.0 ($CH_2CH_2CH_2$).

[Cu$_2$(Me3p)](CF$_3$SO$_3$)$_2$ (5). Me3p (148 mg, 0.269 mmol) was dissolved in CH$_3$OH (50 mL). Over this solution was added [Cu(CH$_3$CN)$_4$]CF$_3$SO$_3$ (202 mg, 0.538 mmol) dissolved in CH$_3$OH (35 mL). The mixture was stirred for 15 min, and the solid that precipitated was filtered and dried under vacuum (170 mg, 65%, 0.174 mmol). FT-IR (KBr): ν = 3450, 1473, 1277, 1260, 1155, 1030, and 637 cm^{-1}. Anal. (%) Calcd for $C_{36}H_{58}N_6Cu_2F_6S_2O_6 \cdot 0.3H_2O$: C 44.05, N 8.56, H 6.02. Found: C 44.01, N 8.46, H 6.04. ^{1}H NMR (CD_3CN, 298 K): δ = 7.28 (s, 8H, arom), 3.48 (s, 8H, $ArCH_2$), 2.57 (m, 16H, NCH_2), 2.38 (s, 6H, NCH_3), 2.24 (s, 12H, NCH_3), 1.81 (m broad, 8H, $CH_2CH_2CH_2$).

[Cu$_2$(Me3m)](CF$_3$SO$_3$)$_2$ (6). Me3m (106 mg, 0.193 mmol) was dissolved in CH$_3$OH (35 mL). Over this solution was added [Cu(CH$_3$CN)$_4$]CF$_3$SO$_3$ (145 mg, 0.385 mmol) dissolved in CH$_3$OH (35 mL). The mixture was stirred for 30 min, and the pale yellow solid that precipitated was filtered and dried under vacuum (165 mg, 81%, 0.156 mmol). FT-IR (KBr): ν = 3450, 1474, 1271, 1252, 1156, 1028, and 638 cm^{-1}. Anal. (%) Calcd for $C_{36}H_{58}N_6Cu_2F_6S_2O_6 \cdot 1.5H_2O$: C 43.10, N 8.38, H 6.13. Found: C 43.08, N 7.97, H 5.78. ^{1}H NMR (DMSO-d_6, 298 K): δ = 7.38 (m broad, 2H, arom), 7.27 (m broad, 6H, arom) 3.54 (s, 8H, $ArCH_2$), 2.49 (t J = 6 Hz, 16H, NCH_2), 2.35−2.22 (m broad, 18H, NCH_3), 1.72 (t J = 6 Hz, 8H, $CH_2CH_2CH_2$).

[Cu$_2$(Me3m)](PF$_6$)$_2$ (7). Me3m (145 mg, 0.263 mmol) was dissolved in CH$_3$OH (5 mL). Over this solution was added [Cu(CH$_3$CN)$_4$]PF$_6$ (197 mg, 0.527 mmol) dissolved in CH$_3$OH (15 mL). The mixture was stirred for 30 min, and the pale yellow solid that precipitated was filtered and dried under vacuum (146 mg, 0.145 mmol, 55%). FT-IR (KBr): ν = 3440, 1475, 846, and 558 cm^{-1}. Anal. (%) Calcd for $C_{34}H_{58}N_6Cu_2P_2F_{12} \cdot 2H_2O$: C 40.68, N 8.37, H 6.22. Found: C 40.65, N 8.31, H 6.12.

[Cu$_2$(Me2p)(CO)$_2$](ClO$_4$)$_2$ (8). Me2p (50 mg, 0.101 mmol) and [Cu(CH$_3$CN)$_4$]ClO$_4$ (66 mg, 0.202 mmol) were dissolved in CH$_3$CN/CH$_3$OH 1:1 v/v (2 mL). The mixture was stirred for 10 min at which time CO was gently bubbled during 5 min. The colorless product that precipitates was filtered and dried under vacuum (72 mg, 0.08 mmol, 81%). FT-IR (KBr): ν = 2087, 1467, 1100, and 625 cm^{-1}. Anal. (%) Calcd for $C_{32}H_{50}N_6Cu_2Cl_2O_{10} \cdot H_2O$: C 42.94, N 9.39, H 5.81. Found: C 43.03, N 9.17, H 5.86. ^{1}H NMR (CD_3CN, 298 K): δ = 8.0−7.0 (m broad, 8H, arom), 4.5−2.1 (m broad, 45H, $ArCH_2$, NCH_2, NCH_3, and H_2O). ^{13}C NMR (CD_3CN, 298 K): δ = 136.3, 132.7, 130.7 (arom), 67.5, 61.7 ($ArCH_2$), 60.4, 54.9, 52.4, 49.4 (NCH_2), 45.7, 43.2 (NCH_3).

[Cu$_2$(Me2m)(CO)$_2$](CF$_3$SO$_3$)$_2$ (9). Me2m (50 mg, 0.101 mmol) and [Cu(CH$_3$CN)$_4$]CF$_3$SO$_3$ (76 mg, 0.202 mmol) were dissolved in CH$_3$CN (2 mL). The mixture was stirred for 10 min after which time CO was gently bubbled for 5 min. The solution was concentrated under vacuum to 0.1 mL. THF (5 mL) saturated with CO was added, and the mixture was left on the fridge. After 24 h, large colorless blocks form, which were filtered and dried under vacuum (79 mg, 0.068 mmol, 67%). FT-IR (KBr): ν = 2087, 1467, 1273, 1151, 1030, and 638 cm^{-1}. Anal. (%) Calcd for $C_{34}H_{50}N_6Cu_2O_8F_6S_2 \cdot 2.5THF$: C 45.74, N 7.28, H 6.11. Found: C 45.77, N 7.11, H 6.10. ^{1}H NMR (CD_3CN, 298 K): δ = 7.85 (s, 2H, arom.), 7.46 (m broad, 6H, arom.), 3.93 (s, 8H, Ar*CH$_2$*), 3.46 (m, 10H, CH_2O THF), 2.83 (m broad, 16H, NCH_2), 2.60 (s, 6H, NCH_3), 2.36 (s, 12H, NCH_3), 2.30 (s, 2H, H_2O), 1.19 (m, 9H, CH_2 THF). ^{13}C NMR (CD_3CN, 298 K): δ = 135.7, 132.8, 130.2, 128.6 (arom), 67.3 (CH_2O THF), 64.7 (Ar*CH$_2$*), 57.3, 53.9 (NCH_2), 45.8, 43.0 (NCH_3), 25.3 (CH_2 THF).

[Cu$_2$(Me2p)(*t*-BuNC)$_2$](ClO$_4$)$_2$ (10). Me2p (50 mg, 0.101 mmol) and [Cu(CH$_3$CN)$_4$]ClO$_4$ (66 mg, 0.202 mmol) were dissolved in CH$_3$CN (2 mL). Over this solution was added *t*-BuNC (23 mg, 0.202 mmol). The solvent was removed under vacuum and the residue recrystallized from CH$_3$CN/THF 5:1 v/v (3 mL) to obtain a white solid (82.7 mg, 0.079 mmol, 78%). FT-IR (KBr): ν = 2165, 1467, 1100, and 625 cm^{-1}. Anal. (%) Calcd for $C_{40}H_{68}N_8Cu_2Cl_2O_8 \cdot H_2O$: C 47.80, N 11.15, H 7.02. Found: C 47.55, N 11.06, H 6.86. ^{1}H NMR (CD_3CN, 338 K): δ = 7.37 (s broad, 8H arom.), 3.74 (s broad, 8H, $ArCH_2$), 2.89 (s broad, 16H, NCH_2), 2.77 (s, 6H, NCH_3), 2.38 (s, 12H, NCH_3), 1.39 (s, 18H, CH_3 isocyanide). ^{13}C NMR (CD_3CN, 298 K): δ = 135.8 (arom ter), 132.6, 130.3 (arom sec), 67.3, 64.0 ($ArCH_2$), 59.6, 57.4, 54.9, 51.7 (NCH_2), 46.7, 42.5 (NCH_3), 29.1 (CH_3 isocyanide).

[Cu$_2$(Me2m)(*t*-BuNC)$_2$](CF$_3$SO$_3$)$_2$ (11). Me2m (50 mg, 0.101 mmol) and [Cu(CH$_3$CN)$_4$]CF$_3$SO$_3$ (76 mg, 0.202 mmol) were dissolved in CH$_3$CN (2 mL). Over this solution was added *t*-BuNC (23 mg, 0.202 mmol) and the mixture stirred for 10 min. The solvent was removed under vacuum and the residue recrystallized from CH$_3$CN/THF 5:1 v/v (3 mL) to obtain very pale blue crystals (59.3 mg, 0.051 mmol, 51%). FT-IR (KBr): ν = 2160, 1471, 1273, 1151, 1030, and 638 cm^{-1}. Anal. (%) Calcd for $C_{42}H_{68}N_8Cu_2F_6S_2O_6 \cdot$ THF: C 47.74, N 9.69, H 6.62. Found: C 48.00, N 9.26, H 6.58. ^{1}H NMR (CD_3CN, 298 K): δ = 7.81 (s, 2H, arom), 7.48 (broad, 6H, arom), 4.00 (s, 8H, Ar*CH$_2$*), 2.81 (m broad, 16H, NCH_2), 2.43 (s, 6H, NCH_3), 2.32 (s, 12H, NCH_3), 2.21 (s, 3H, H_2O), 1.34 (s,

18 H, CH_3 isocyanide). ^{13}C NMR (CD_3CN, 298 K): δ = 130.0, 128.5 (arom), 65.1, 64.7 (ArCH_2), 57.2, 54.3 (NCH_2), 46.9, 42.6 (NCH_3), 29.3 (CH_3 isocyanide).

$[Cu_2(Me2p)(PPh_3)_2](ClO_4)_2$ (12). Me2p (50 mg, 0.101 mmol) and $[Cu(CH_3CN)_4]ClO_4$ (66 mg, 0.202 mmol) were dissolved in acetone (5 mL). Over this solution was added PPh_3 (0.202 mmol, 53 mg) dissolved in acetone (3 mL). A white precipitate rapidly appears which is filtered, washed with acetone, and dried under vacuum (108 mg, 0.08 mmol, 79%). FT-IR (KBr): ν = 1467, 1495, 1100, and 625 cm^{-1}. Anal. (%) Calcd for $C_{66}H_{80}N_6Cu_2P_2Cl_2O_8$: C 59.00, N 6.26, H 6.01. Found: C 58.16, N 6.37, H 6.01. ^1H NMR (CD_3CN, 298 K): δ = 7.54−7.29 (m, 38H, arom.), 3.58 (s, 8H, ArCH_2), 2.97−2.63 (m, 16H, NCH_2), 2.25 (s, 12H, NCH_3), 2.13 (s, NCH_3).^1H NMR (DMSO-d_6, 298 K): δ = 7.54−7.10 (m, 38H), 3.52 (s, 8H), 2.7−2.5 (m, 16H), 2.34 (s, 6H), 2.27 (s, 9H), 2.1 (s, 4H). ^{13}C NMR (DMSO-d_6, 298 K): δ = 134.0, 133.3, 133.1, 132.3, 131.6, 130.6, 129.8, 129.3, 129.1 (arom), 63.5, 54.5 (ArCH_2), 45.0, 43.6 (NCH_2), 30.7 (NCH_3). ^{31}P NMR (DMSO-d_6, 298 K): δ = 1.1, $\Delta\delta$ = 10 ppm.

$[Cu_2(Me2m)(PPh_3)_2](ClO_4)_2$ (13). Me2m (50 mg, 0.101 mmol) and $[Cu(CH_3CN)_4]ClO_4$ (66 mg, 0.202 mmol) were dissolved in acetone (5 mL). Over this solution was added PPh_3 (0.202 mmol, 53 mg) dissolved in acetone (3 mL). A white precipitate rapidly appeared which was filtered, washed with acetone, and dried under vacuum (111 mg, 0.08 mmol, 82%). FT-IR (KBr): ν = 1467, 1495, 1091, and 620 cm^{-1}. Anal. (%) Calcd for $C_{66}H_{60}N_6Cu_2Cl_2O_8 \cdot CH_3CN \cdot 1.5H_2O$: C 57.78, N 6.94, H 6.13. Found: C 57.55, N 6.93, H 5.90. ^1H NMR (CD_3CN, 298 K): δ = 7.54−7.29 (m, 38H, arom), 3.75 (s., 8H, ArCH_2), 2.68 (m broad, 16H, NCH_2), 2.40 (s, broad, 6H, NCH_3), 2.27 (s, 12H, NCH_3). ^1H NMR (DMSO-d_6 298 K): δ = 7.6−7.4 (m, 38H, arom.), 3.6 (s, 8H, ArCH_2), 2.7−2.1 (m, 34H, NCH_2 and NCH_3). ^{13}C NMR (CD_3CN, 298 K): δ = 133.5, 133.2, 132.8, 132.2, 131.6, 130.3, 129.0, 128.9, 127.9, 117.3 (arom), 63.1 (ArCH_2), 54.7, 54.5 (NCH_2), 42.4 (NCH_3).^{31}P NMR (DMSO-d_6): δ = 0.0, $\Delta\delta$ = 10 ppm.

Physical Methods. IR spectra were taken in a Mattson-Galaxy Satellite FT-IR spectrophotometer as solid KBr pellets. Elemental analyses were conducted in a Carlo Erba Instrument, model CHNS 1108. NMR spectra were recorded on a Bruker DPX-200 operating at 200.13 MHz for ^1H, 50.32 MHz for ^{13}C, and 80.01 MHz for ^{31}P, at room temperature (298 K), or on a BRUKER ARX400 spectrometer operating at 400.13 MHz for proton, equipped with a 5 mm triple-resonance inverse broadband probe head and a *z*-gradient coil. 2D COSY and HSQC experiments were recorded using standard pulse sequences, and 2D NOESY spectra using a mixing time of 500 ms were obtained at several temperatures to identify NOEs and chemical exchange cross-peaks. Spectra were referenced to the residual protio solvents peaks or TMS (tetramethylsilane) for ^1H and to external H_3PO_4 (85%) for ^{31}P.

Crystallographic Studies. $[Cu_2(Me2p)(CO)_2](ClO_4)_2 \cdot 2H_2O$ (8). A colorless cube with the dimensions 0.10 × 0.15 × 0.25 mm^3 was coated with a viscous oil, stuck with glue on a glass fiber, and mounted on the diffractometer equipped with an Oxford Cryostream low temperature device. Unit cell parameters were determined by carefully centering 25 independent, strong reflections with 14° ≤ θ ≤ 23°. Data collection has been carried out at 193 K using a Enraf-nonius CAD4 diffractometer equipped with a Cu Kα fine focus sealed tube (λ = 1.54180 Å) and with a graphite monochromator. 6433 reflections with 2.42° ≤ 2θ ≤ 77.50° were measured. Three reflections monitored every 2 h showed an intensity loss of 6.12%. Absorption correction was carried out using DIFABS[38] (minimum and maximum transmission: 0.60/1.00). The structure was solved by direct methods using the program SIR92.[39] Anisotropic least-squares full-matrix refinement was carried out on all non-hydrogen atoms using the program CRYSTALS.[40] The hydrogen atoms are in calculated positions. The protons of the water of crystallization could not be localized. The refinement of 487 parameters including 3350 reflections with $I > 3\sigma(I)$ lead to a residual of 0.0588 (R_w = 0.0613). Chebychev polynomial weights[41] have been used to complete the refinement. The density maximum in the last difference map was 0.94 e/Å^3, and the last minimum was −0.76 e/Å^3. Scattering factors have been taken from the International Tables, Vol. IV, Table 2.2B.

$[Cu_2(Me2m)(t\text{-}BuNC)_2](CF_3SO_3)_2$ (11). A pale blue rod crystal was coated with a viscous oil, stuck with glue on the end of a glass fiber, and mounted on the diffractometer. The intensity data were collected at 223 K on a Stoe image plate diffraction system[42] using Mo Kα graphite monochromated radiation: image plate distance 70 mm, ϕ oscillation scans 0−200°, step $\Delta\phi$ = 1.0°, 2θ range 3.27−52.1°, $d_{max}-d_{min}$ = 12.45−0.81 Å. The structure was solved by direct methods using the program SHELXS-97.[43] The refinement and all further calculations were carried out using SHELXL-97.[44] The H-atoms were included in calculated positions and treated as riding atoms using SHELXL default parameters. The non-H atoms were refined anisotropically, using weighted full-matrix least-squares on F^2. An empirical absorption correction was applied using the DIFABS routine in PLATON[38] (transmission min/max = 0.452/0.820). One of the triflate anions undergoes considerable thermal motion.

CCDC 190908 and 190909 contain the supplementary crystallographic data for complexes $[Cu_2(Me2m)(t\text{-}BuNC)_2](CF_3SO_3)_2$, **11**, and $[Cu_2(Me2p)(CO)_2](ClO_4)_2 \cdot 2H_2O$, **8**, respectively, described in this paper. These data can be obtained free of charge via www.ccdc.cam.uk/conts/retrieving.html (or from the Cambridge Crystallographic Data Center, 12 Union Road, Cambridge CB2 1EZ, U.K. Fax: (+44)1223-336-033. E-mail: deposit@ccdc.cam.ac.uk.).

Computational Details. The reported calculations were carried out by using the Amsterdam density functional (ADF) program system, developed by Baerends et al.[45−47] The numerical integration scheme employed was that of te Velde and Baerends.[48] An uncontracted triple-ζ basis set[49] was used for describing the 3s, 3p, 3d, 4s, and 4p orbitals of copper. For carbon (2s,2p), nitrogen (2s,-2p), oxygen (2s,2p), and hydrogen (1s), double-ζ basis sets[49] were

(38) *DIFABS*: Walker, N.; Stuart, D. *Acta Crystallogr., Sect. A* **1983**, *39*, 158−166.
(39) *SIR92*: Altomare, A.; Cascarano, G.; Giacovazzo, G.; Guagliardi, A.; Burla, M. C.; Polidori, G.; Camalli, M. *J. Appl. Crystallogr.* **1994**, *27*, 435.
(40) *CRYSTALS*: Watkin, D. J.; Carruthers, R. J.; Betteridge, P. *CRYSTALS*; Chemical Crystallography Laboratory: Oxford, U.K., 1985.
(41) Carruthers, J. R.; Watkin, D. J. *Acta Crystallogr., Sect. A* **1979**, *35*, 698−699.
(42) *Stoe & Cie IPDS Software*; Stoe & Cie GmbH: Germany, 2000.
(43) *SHELXS-97*: Sheldrick, G. *Acta Crystallogr., Sect. A* **1990**, *46*, 467−473.
(44) *SHELXS-97*: Sheldrick, G. *SHELXS-97*; Universität Göttingen: Göttingen, Germany, 1999.
(45) te Velde, G.; Bickelhaupt, F. M.; Baerends, E. J.; Fonseca Guerra, C.; Van Gisbergen, S. J. A.; Snijders, G. J.; Ziegler, T. *J. Comput. Chem.* **2001**, *22*, 931−967.
(46) (a) Baerends, E. J.; Ellis, D. E.; Ros, P. *Chem. Phys.* **1973**, *2*, 41−51. (b) Baerends, E. J. Ph.D. Thesis, Vrije Universiteit, Amsterdam, 1975.
(47) Ravenek W. In *Algorithms and Applications on Vector and Parallel Computers*; te Riele, H. J. J., Dekker, Th. J., van de Vorst, H. A., Eds.; Elsevier: Amsterdam, 1987.
(48) te Velde, G. B.; Baerends, E. J. *J. Comput. Phys.* **1992**, *99*, 84−98.
(49) (a) Snijders, G. J.; Baerends, E. J.; Vernooijs, P. *At. Nucl. Data Tables* **1982**, *26*, 483. (b) Vernooijs, P.; Snijders, G. J.; Baerends, E. J. *Slater Type Basis Functions for the Whole Periodic System. Internal Report*; Vrije Universiteit of Amsterdam: Amsterdam, The Netherlands, 1981.

employed and augmented by an extra polarization function. Electrons in lower shells were treated within the frozen core approximation.[46a] A set of auxiliary s, p, d, f, and g functions,[50] centered in all nuclei, was introduced in order to fit the molecular density and Coulomb potential accurately in each SCF cycle. Geometries were fully optimized within the local density approximation (LDA), which includes the X_α exchange ($\alpha = {}^2/_3$),[51] together with the electron gas correlation functional in the Vosko−Wilk−Nusair parametrization.[52] The analytical gradients implemented by Versluis and Ziegler[53] were employed to perform geometry optimizations. Energies were evaluated at the LDA molecular geometries using a generalized gradient approximation (GGA) that includes the nonlocal exchange correction of Becke[54] and the nonlocal correlation correction of Perdew.[55] This method is labeled throughout this work as BP86/DZP//VWN/DZP. Several authors have shown that this level of calculation provides excellent results for geometries and bond dissociation energies.[56−61]

Owing to computational limitations, both geometry optimizations and energy evaluations have been carried out with the QM/MM method available in the ADF program, which includes standard molecular mechanics force fields in such a way that the QM and MM parts are coupled self-consistently.[62] In the QM/MM model considered in this work, the MM part involves the two aromatic rings in the ligand and the four CH_2 units of the benzylic groups. As for the connection between the QM and MM parts, this occurs by means of the so-called "capping" dummy hydrogen atoms, which are replaced in the real system by the corresponding "linking" carbon atoms.[62,63] In the QM/MM optimizations, the ratio between the C−N bonds crossing the QM/MM border, and the corresponding optimized C−H distances, was fixed equal to 1.38. A more detailed description of the coupling scheme, as well as further comments on the methodology, can be found in previous papers.[63−65] The AMBER95 force field[66] was used for the MM potentials, except for Cu, which was treated with the UFF force field.[67] To eliminate spurious stabilizations from the long-range attractive part of the Lennard-Jones potential,[65,68] we used an exponential expression fitted to the repulsive part of the Lennard-Jones potential.[65,69−71] The QM/MM scheme in the ADF program has been successfully employed to investigate olefin polymerizations,[64,72] epoxidation of olefins,[73] and rhodium catalyzed carbonylation reactions.[74] The 2000.02 release of the ADF package was used for all calculations.[75]

Scheme 1. Macrocyclic Ligands Used in This Work

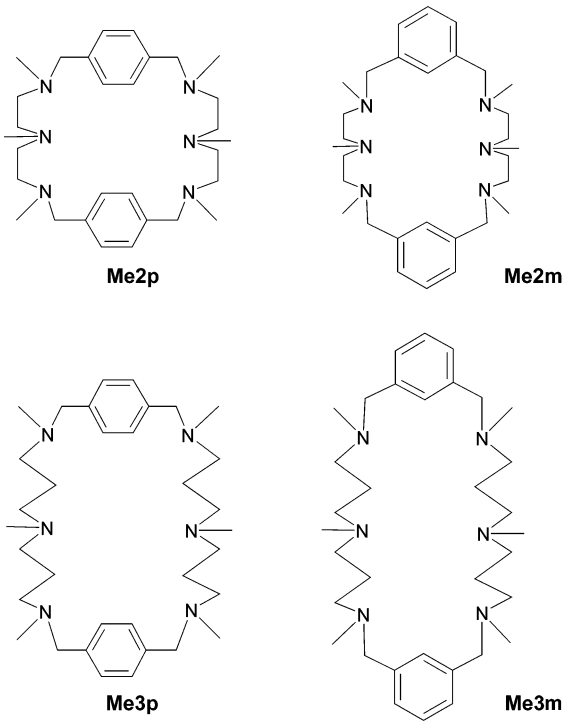

Results

Synthesis. The four macrocyclic ligands used in this work are represented in Scheme 1 and are prepared according to literature procedures. This family of ligands is characterized by the number of methylenic units linking the tertiary amines, which can be two or three, and by the aromatic substitution that take place in the *meta* or *para* positions. Reaction of those ligands containing two methylenic units (Me2p and Me2m) with 2 equiv of $[Cu(CH_3CN)_4]X$ ($X^- = ClO_4^-$, $CF_3SO_3^-$, or PF_6^-) in acetonitrile form the corresponding dinuclear complexes, in moderate to good yields, as shown in the following equation for the case of Me2p.

$$\text{Me2p} + 2\ \text{Cu(MeCN)}_4{}^{+} \xrightarrow{\text{MeCN}} \underset{\mathbf{1}}{[\text{Cu}_2(\text{Me2p})(\text{MeCN})_2]^{2+}} + 6\ \text{MeCN} \quad (1)$$

The complexes thus obtained are white solids, which are air sensitive. The replacement of MeCN by *n*-PrCN in this

(50) Krijn, J. B.; Baerends, E. J. *Fit functions in the HFS method.*; Internal Report; Vrije Universiteit of Amsterdam: Amsterdam, The Netherlands, 1984.
(51) Slater, J. C. *Quantum Theory of Molecules and Solids, Vol. 4*; McGraw-Hill: New York, 1974.
(52) Vosko, S. H.; Wilk, L.; Nusair, M. *Can. J. Phys.* **1980**, *58*, 1200−1211.
(53) Versluis, L.; Ziegler, T. *J. Chem. Phys.* **1988**, *28*, 322−328.
(54) Becke, A. D. *Phys. Rev. A* **1988**, *38*, 3089−3100.
(55) Perdew, J. P. *Phys. Rev. B* **1986**, *33*, 8822−8824.
(56) Li, J.; Schreckenback, G.; Ziegler, T. *J. Phys. Chem.* **1994**, *98*, 4838−4841.
(57) Bickelhaupt, F. M.; Solà, M.; Schleyer, P. v. R. *J. Comput. Chem.* **1995**, *16*, 465−477.
(58) Torrent, M.; Deng, L.; Duran, M.; Solà, M.; Ziegler, T. *Organometallics* **1997**, *16*, 13−19.
(59) Torrent, M.; Deng, L.; Duran, M.; Solà, M.; Ziegler, T. *Can. J. Chem.* **1999**, *77*, 1476−1491.
(60) Deng, L.; Ziegler, T. *Organometallics* **1997**, *16*, 716−724.
(61) Deng, L.; Ziegler, T. *Organometallics* **1996**, *15*, 3011−3021.
(62) Maseras, F.; Morokuma, K. *J. Comput. Chem.* **1995**, *16*, 1170−1179.
(63) Woo, T. K.; Cavallo, L.; Ziegler, T. *Theor. Chem. Acc.* **1998**, *100*, 307−313.
(64) Deng, L.; Woo, T. K.; Cavallo, L.; Margl, P. M.; Ziegler, T. *J. Am. Chem. Soc.* **1997**, *119*, 6177−6186.
(65) Cavallo, L.; Woo, T. K.; Ziegler, T. *Can. J. Chem.* **1998**, *76*, 1457−1466.
(66) Cornell, W. D.; Cieplak, P.; Bayly, C. I.; Gould, I. R.; Merz, K. M. J.; Ferguson, D. M.; Spellmeyer, D. C.; Fox, T.; Caldwell, J. W.; Kolmann, P. A. *J. Am. Chem. Soc.* **1995**, *117*, 5179−5197.
(67) Rappé, A. K.; Casewit, C. J.; Colwell, K. S.; Goddard, W. A., III; Shiff, W. M. *J. Am. Chem. Soc.* **1992**, *114*, 10024−10035.
(68) Sauers, R. R. *J. Chem. Educ.* **1996**, *73*, 114−116.
(69) Lee, K. J.; Brown, T. L. *Inorg. Chem.* **1992**, *31*, 289−294.
(70) Woo, T. K.; Ziegler, T. *Inorg. Chem.* **1994**, *33*, 1857−1863.
(71) Guerra, G.; Cavallo, L.; Corradini, P.; Longo, P.; Resconi, L. *J. Am. Chem. Soc.* **1997**, *119*, 4394−4403.
(72) Guerra, G.; Longo, P.; Corradini, P.; Cavallo, L. *J. Am. Chem. Soc.* **1999**, *121*, 8651−8652.
(73) Jacobsen, H.; Cavallo, L. *Chem. Eur. J.* **2001**, *7*, 800−807.
(74) Cavallo, L.; Solà, M. *J. Am. Chem. Soc.* **2001**, *123*, 12294−12302.
(75) *ADF 2000*; Vrije Universiteit Amsterdam: Amsterdam, The Netherlands, 2000.

reaction generates the corresponding complexes, $[Cu_2(Me2p)(n\text{-}PrCN)_2](ClO_4)_2$, **2**, and $[Cu_2(Me2m)(n\text{-}PrCN)_2](PF_6)_2$, **3**, which are less air sensitive and thus easier to manipulate. For the analogous ligands with three methylenic units, Me3p and Me3m, the metal centers in $[Cu_2(Me3p)](ClO_4)_2$, **4**, $[Cu_2(Me3p)](CF_3SO_3)_2$, **5,** $[Cu_2(Me3m)](CF_3SO_3)_2$, **6**, and $[Cu_2(Me3m)](PF_6)_2$, **7**, are solely coordinated by the macrocyclic ligand, and therefore, a three coordination is obtained. This statement is supported analytically and spectroscopically by the absence of a nitrile band in the IR and the absence of the corresponding resonances in the NMR. Furthermore, the alkyltriamine moieties in the Me3p and Me3m ligands are almost identical to those in the recently crystallographically characterized $[Cu^I(MeAN)]B(C_6F_5)_4$ (MeAN = *N*,*N*′,*N*′,*N*″-pentamethyldipropylenetriamine)[29] which also possesses a tricoordinate copper(I) center, even when isolated from acetonitrile as solvent.

For the dinuclear copper complexes containing the isomeric ligands with two methylenic units bonding tertiary amines, Me2p and Me2m, their monodentate ligand can easily be replaced by σ-donor/π-acceptor ligands L (CO, *t*-BuNC, PPh_3) as shown here for the particular case of Me2p:

$$\underset{\mathbf{1}}{[Cu_2(Me2p)(MeCN)_2]^{2+}} + 2\ L \xrightarrow{MeCN} [Cu_2(Me2p)L_2]^{2+} + 2\ MeCN \quad (2)$$

These new complexes are generally obtained in good yields, precipitate as white solids, and are less air sensitive than their precursors. However, the stability of the complexes is somewhat dependent on the σ-donor/π-acceptor ligands L. Carbonyl complexes $[Cu_2(Me2p)(CO)_2](ClO_4)_2$, **8**, and $[Cu_2(Me2m)(CO)_2](CF_3SO_3)_2$, **9**, are rapidly oxidized in the solid-state and in solution upon exposure to O_2, PPh_3 complexes $[Cu_2(Me2p)(PPh_3)_2](ClO_4)_2$, **12**, and $[Cu_2(Me2m)(PPh_3)_2](ClO_4)_2$, **13**, are relatively stable in the solid-state but become oxidized in O_2 exposed solutions, and acetonitrile solutions of *t*-BuNC complexes $[Cu_2(Me2p)(t\text{-}BuNC)_2](ClO_4)_2$, **10**, and $[Cu_2(Me2m)(t\text{-}BuNC)_2](CF_3SO_3)_2$, **11**, could be manipulated in open atmosphere for short periods of time without apparent oxidation of the complexes.

The corresponding complexes containing the isomeric ligands Me3p and Me3m are also formed using acetone as the solvent, as evidenced by IR spectroscopy, but they cannot be isolated in the solid-state. In the workup process, the corresponding σ-donor/π-acceptor ligand is lost, thus generating the tricoordinated complexes. Furthermore, in the particular case of the complexes containing the carbonyl ligand, the established equilibrium process can be monitored by IR spectroscopy indicating the reversibility of the process in solution:

$$[Cu_2(Me3p)(MeCN)_2]^{2+} + 2\ CO \underset{MeCN}{\overset{CO}{\rightleftharpoons}} [Cu_2(Me3p)(CO)_2]^{2+} + 2\ MeCN \quad (3)$$

The reaction is driven to the left by simply bubbling Ar or N_2 into the solution at room temperature.

Table 1. Crystallographic Data of $[Cu_2(Me2p)(CO)_2](ClO_4)_2 \cdot 2H_2O$, **8**, and $[Cu_2(Me2m)(t\text{-}BuNC)_2](CF_3SO_3)_2$, **11**

	8	**11**
formula	$C_{32}H_{54}Cl_2Cu_2N_6O_{12}$	$C_{42}H_{68}Cu_2F_6N_8O_6S_2$
MW [g/mol]	912.80	1086.24
cryst syst	monoclinic	orthorhombic
space group	$P2_1/n$	*Pbca*
a [Å]	14.973(2)	16.8695(9)
b [Å]	14.744(4)	22.3450(14)
c [Å]	18.374(2)	27.3252(17))
β [deg]	95.31(1)	90.00(1)
V [Å^3]	4039(1)	10300.2(11)
Z	4	8
T [K]	193(2)	223(2)
radiation used	Cu Kα, 1.54180 Å	Mo Kα, 0.71073 Å
ρ_{calcd} [g/cm^3]	1.501	1.401
μ, [mm^{-1}]	3.07	0.979
T_{max}/T_{min}	1.00/0.60	0.820/0.452
cryst form	cube	rod
cryst size [mm^3]	0.10 × 0.15 × 0.25	0.08 × 0.10 × 0.30
$2\theta_{max}$ [deg]	77.50	52.1
no. reflns	6433	78116
no. indep reflns	6113	10036
no. obsd reflns	3350 ($I > 3\sigma(I)$)	3803 ($I > 2\sigma(I)$)
restrains/params	0/487	0/589
final *R*	0.0588	0.0555
final R_w	0.0613	0.1277
max/min in diff map [e Å^{-3}]	0.94/−0.76	0.988/−0.640

Table 2. Selected Bond Lengths (Å) and Bond Angles (deg) for $[Cu_2(Me2p)(CO)_2](ClO_4)_2$, **8**, and $[Cu_2(Me2m)(t\text{-}BuNC)_2](CF_3SO_3)_2$, **11**

Complex **8**

	X-ray	calcd		X-ray	calcd
Cu1−N1	2.166(5)	2.142	Cu51−N53	2.173(6)	2.140
Cu1−N2	2.109(6)	2.052	Cu51−N52	2.086(6)	2.044
Cu1−N3	2.115(6)	2.121	Cu51−N51	2.106(6)	2.145
Cu1−C4	1.813(8)	1.784	Cu51−C54	1.815(8)	1.781
C4−O5	1.113(9)	1.142	C54−O55	1.114(9)	1.142
Cu1−C4−O5	176.4(8)	172.9	Cu51−C54−O55	176.2(2)	173.3
N1−Cu1−N2	85.9(2)	85.3	N52−Cu51−N53	85.6(2)	85.7
N1−Cu1−N3	114.0(2)	117.1	N51−Cu51−N53	115.4(2)	115.1
N2−Cu1−N3	87.0(2)	87.1	N51−Cu51−N52	87.2(3)	86.9
N1−Cu1−C4	112.8(3)	109.5	N53−Cu51−C54	110.3(3)	110.1
N2−Cu1−C4	122.9(3)	132.9	N52−Cu51−C54	123.3(3)	134.7
N3−Cu1−C4	125.3(3)	120.4	N51−Cu51−C54	126.5(3)	119.8
Cu1···Cu51	6.810	7.226	O5···O55	3.122	2.961
C4O5−O55C54	−5.3	2.6			

Complex **11**

	X-ray		X-ray
Cu1···Cu2	6.776	Cu2−C36	1.836(2)
Cu1−C31	1.832(6)	Cu2−N6	2.102(5)
Cu1−N2	2.100(5)	Cu2−N5	2.169(5)
Cu1−N1	2.176(5)	Cu2−N7	2.231(5)
Cu1−N3	2.181(4)	C36−Cu2−N6	135.9(2)
C31−Cu1−N2	130.6(2)	C36−Cu2−N5	115.6(2)
C31−Cu1−N1	111.5(2)	N6−Cu2−N5	85.50(19)
N2−Cu1−N1	85.8(2)	C36−Cu2−N7	114.3(2)
C31−Cu1−N3	120.2(2)	N6−Cu2−N7	85.2(2)
N2−Cu1−N3	85.29(17)	N5−Cu2−N7	116.07(18)
N1−Cu1−N3	118.12(17)		

Structure. The crystal structures of complexes $[Cu_2(Me2p)(CO)_2](ClO_4)_2 \cdot 2H_2O$, **8**$\cdot 2H_2O$, and $[Cu_2(Me2m)(t\text{-}BuNC)_2](CF_3SO_3)_2$, **11**, have been determined by means of single-crystal X-ray diffraction analysis. Table 1 contains crystallographic data for complexes **8** and **11**, whereas Table 2 contains their selected bond distances and angles. Figure 1 displays the ORTEP diagrams obtained for the cationic molecular structures of complexes **8** and **11** which crystallize

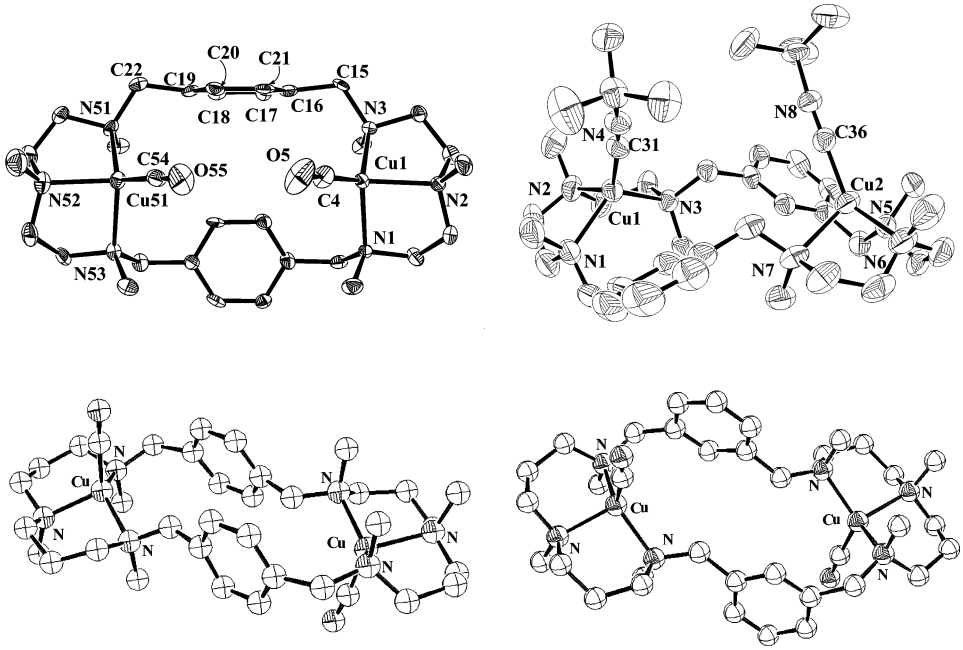

Figure 1. ORTEP diagram (50% probability) of the cationic part of complex $[Cu_2(Me2p)(CO)_2](ClO_4)_2$, **8**, (top left) and of complex $[Cu_2(Me2m)(t\text{-BuNC})_2](CF_3SO_3)_2$, **11**, (top right). Calculated structures using DFT for complexes *anti*-$[Cu_2(Me3p)(CO)_2]^{2+}$ (bottom left) and *anti*-$[Cu_2(Me3m)(CO)_2]^{2+}$ (bottom right). Calculated structures of *syn*-$[Cu_2(Me3p)(CO)_2]^{2+}$ and *syn*-$[Cu_2(Me3m)(CO)_2]^{2+}$ are −1.7 and −1.8 kcal/mol less stable, respectively, than the corresponding anti forms (see text for details).

in the monoclinic $P2_1/n$ and the orthorhombic *Pbca* space groups with four and eight molecules per unit cell, respectively.

The cationic part of **8** consists of the macrocyclic ligand, binding two copper atoms and two CO molecules acting in a terminal mode. It has a pseudo-plane-of-symmetry that bisects the two aromatic rings and is also perpendicular to them, thus generating two very similar halves of the cationic molecule. The copper atoms have a significantly distorted tetrahedral coordination. Each one is bound to three N atoms of the macrocycle, and a CO molecule completes the coordination sphere. Two of the three Cu1−N distances in **8** are significantly shorter than the other: 2.109(6) and 2.115(6) versus 2.166(5) Å, although all the values lie in the range of Cu−N distances reported in the literature for related copper(I) complexes with alkylated amines.[29,76−79] The bond angles associated with the copper center allow us to grasp the type and degree of tetrahedral distortion suffered by the metal center. Two of the NCuN angles are close to 90° (N1−Cu1−N2, 85.9(2)° and N2−Cu1−N3, 87.0(2)°) whereas the third is slightly above the ideal 109.47° for a tetrahedral geometry (N1−Cu1−N3, 114.0(2)°). The Cu−CO distance is 1.813(8) Å, and the C4−O5 is 1.113(9) Å, both indicative of a weak bonding interaction. In addition, the Cu−CO vector is bent toward N1 (C4−Cu1−N1, 112.8°) resulting in the opening of the C4−Cu1−N2 and C4−Cu1−N3 angles (122.9° and 125.3°, respectively). The aromatic rings are oriented almost perpendicular to each other (80.71°), and the benzylic CH_2 groups are slightly displaced from the plane defined by these aromatic rings. This is evidenced by the C20−C21−C16−C15 and C17−C18−C19−C22 torsion angles of 172.8° and 171.0°, respectively, which indicate the degree of constrain supported by the molecule. Cu−CO vectors point in the same direction (syn) relative to the cavity plane of the macrocyclic ligand with a torsion angle between CO ligands, C4−O5−O55−C54 of −5.3°.

The structure of **8** is completed with two water molecules and two perchlorate anions. One of the water molecules is bonded to one of the perchlorates via hydrogen bonding: O102−O12 is 2.906 Å.

The cationic part of $[Cu_2(Me2m)(t\text{-BuNC})_2](CF_3SO_3)_2$, **11**, consists also of the macrocyclic ligand binding the two metal centers and two *t*-BuNC molecules acting in a terminal fashion (see Figure 1). The cationic moiety possesses a pseudo-C_2 axis perpendicular to the macrocyclic cavity. However, subtle differences between the structural parameters of the two copper centers are evident in **11**. The local geometry around the metal center is relatively similar to that in the case of **8**. Cu(1) has two long Cu−N distances (Cu1−N1 = 2.176(5) Å and Cu1−N3 = 2.181(4) Å) and a shorter one (Cu1−N2 = 2.100(5) Å) whereas Cu2 has three different Cu−N distances (Cu2−N5 = 2.169(5) Å, Cu2−N6 = 2.102(5) Å, and Cu2−N7 = 2.231(5) Å). The NCuN angles are similar to the previous case and thus reflect a relatively similar type of geometrical distortion for the local copper(I) center. Cu−C bonds in Cu−C≡N are short (Cu−C≡N_{av} = 1.83 Å) and compare well with the shortest reported in the literature.[80−84] In addition, the Cu−CN vectors point in the

(76) Pascuali, M.; Floriani, C.; Gaetani-Manfredotti, A.; Villa, A. C. *Inorg. Chem.* **1979**, *18*, 3535−3542.
(77) Scott, M. J.; Holm, R. H. *J. Am. Chem. Soc.* **1994**, *116*, 11357−11367.
(78) Hubin, T. J.; Alcock, N. W.; Busch, D. H. *Acta Crystallogr., Sect. C.* **2000**, *56*, 37.
(79) Becker, M.; Heinemann, F. W.; Knoch, F.; Donaubauer, W.; Liehr, G.; Schindler, S.; Golub, G.; Cohen, H.; Meyerstein, D. *Eur. J. Inorg. Chem.* **2000**, 719−726.

Table 3. Energy of the Syn and Anti Cu−CO Complexes Taking the *syn* System as the Reference Species at Zero Energy, C−O Bond Length of the CO Molecule in the Complex, and Deformation, Interaction, and Bond Coordination Energies of a CO Molecule to the Complex. Bond Distances in Å and Energies in kcal·mol^{-1}

	Me2p		Me2m		Me3p		Me3m	
	syn	anti	syn	anti	syn	anti	syn	anti
ΔE	0.0	7.6	0.0	5.4	0.0	−1.7	0.0	−1.8
r(C−O)[a]	1.142	1.136	1.142	1.137	1.140	1.139	1.141	1.138
ΔE_{CO}	−28.3	−20.3	−25.0	−21.0	−11.1	−12.4	−2.9	−10.9
ΔE_{def}(CO)[b]	−0.1	−0.1	−0.1	−0.1	−0.1	−0.1	−0.1	−0.1
ΔE_{def}(rest)[c]	7.1	10.3	9.1	13.4	13.0	12.0	22.3	15.9
ΔE_{def}[d]	7.0	10.2	9.0	13.3	12.9	11.9	22.2	15.8
ΔE_{int}	−35.3	−30.5	−34.0	−34.3	−24.5	−24.2	−25.15	−26.7

[a] Calculated r(CO) distance in free CO is 1.131 Å, the experimental X-ray value being 1.128 Å.[86] [b] Deformation energy of the CO molecule in the $[Cu_2L(CO)_2]^{2+}$ complex. [c] Deformation energy of the $[Cu_2L(CO)]^{2+}$ without a CO molecule fragment in the $[Cu_2L(CO)_2]^{2+}$ complex. The energy of this fragment can be different for the syn and anti isomers. [d] Total deformation energy, $\Delta E_{def} = \Delta E_{def}(CO) + \Delta E_{def}(rest)$.

same direction (syn) relative to the cavity plane of the[83] macrocyclic ligand with a torsion angle between *t*-BuNC ligands (C31N4−N8C36) of −69.7°. The aromatic rings form a dihedral angle of 52.1°. The structure of **11** is completed with two trifluoromethanesulfonate anions.

The X-ray structures of **8** and **11** are in good agreement with the structures in solution determined by ^{1}H NMR at low temperature (vide infra).

Theoretical Calculations. ADF theoretical calculations were performed for the whole family of dicarbonyl dicopper complexes containing the four ligands described in Scheme 1 in the syn and anti conformations. The energetic results obtained from the computational experiments are summarized in Table 3. The structural drawings and selected bond distances and angles are displayed in Figure 1 and in Table 2, respectively. Cartesian atomic coordinates for all the calculated complexes are included in the Supporting Information.

Due to the presence of the methyl groups coordinated to nitrogen atoms that can adopt up and down positions and because of the boat and chair conformations of the methylene chain connecting nitrogen atoms in the ligand, a large number of possible conformers for each isomer are possible. Since available computational resources do not allow for a complete study of all possible conformers, a single conformer for each isomer was studied. For the *syn*-$[Cu_2(Me2p)(CO)_2]^{2+}$, *syn*-**8**, complex, we started the geometry optimization from the available X-ray coordinates. In turn, the anti complex was optimized from the syn optimized form by taking one of the two QM fragments (the xylylic part of the molecule) and turning it upside down. No further conformational analyses were carried out in this work.

The theoretically calculated structure for *syn*-$[Cu_2(Me2p)(CO)_2]^{2+}$, *syn*-**8**, is remarkably similar to that of the X-ray structure described in the previous section. The highest discrepancy between calculated and experimental metal−ligand bond distances is only 0.057 Å with a medium discrepancy of 0.026 Å (see Table 2). As expected, the main differences are found in the bonding angles; while most of the bonding angle discrepancies are roughly around only 3°, in this case the N2−Cu1−C4 discrepancy is of 10° which could even be ascribed to packing effects. Therefore, a very good agreement is found between the experimental and theoretical bond lengths and angles, thus providing confidence in the reliability of the QM/MM method to reproduce the geometries for this kind of complex.

The theoretical C−O triple bond in the CO free molecule (1.131 Å) is smaller than that of the coordinated CO at the complex (1.142 Å), as expected from the bonding mechanism that usually operates in M−CO bonds.[85] Surprisingly, this is not reproduced by the experimental data since, experimentally, the C−O bond length in CO free molecule is 1.128 Å[86a] and the X-ray data show that in the *syn*-$[Cu_2(Me2p)(CO)_2]^{2+}$, *syn*-**8**, complex this bond length is shorter by 0.014 Å (1.114 Å). It is worth noting that we found previously a similar behavior for the experimental and theoretical triple bond lengths of the CO and CNCN ligands in the $Cr(CO)_5$CNCN system.[86b] We have not been able to find an explanation for this discrepancy, although the expected lengthening and weakening of the CO bond in the complex fits in with the generally observed IR frequency lowering of the CO stretch vibration.

The energy difference between the *syn*- and *anti*-$[Cu_2(Me2p)(CO)_2]^{2+}$, **8**, complexes is listed in Table 3. In agreement with the experimental findings, we found that the *syn*-$[Cu_2(Me2p)(CO)_2]^{2+}$, *syn*-**8**, complex is more stable than the anti complex by 7.6 kcal mol^{-1} at the QM(BP86/DZP//VWN/DZP)/MM(AMBER95) level of theory.

In order to gain further insight into the different parameters that govern the relative stability of these complexes, their CO coordination energies were also calculated.

$$[Cu_2Mac(CO)]^{2+} + CO \rightleftarrows [Cu_2(Mac)(CO)_2]^{2+} \qquad (4)$$

The bond coordination energy of CO has been divided into deformation energy and interaction energy ($\Delta E_{CO} = \Delta E_{def} + \Delta E_{int}$). The deformation energy is the energy needed to modify the geometry of the free fragments to attain the geometry that they have in the complex, and it is split into the deformation of the CO molecule (ΔE_{def}(CO)) and the deformation of the rest of the complex (ΔE_{def}(rest)). The interaction energy is the energy released when the two free deformed fragments are brought to the position that they have in the complex.

In agreement with the higher stability of the *syn*-$[Cu_2(Me2p)(CO)_2]^{2+}$, *syn*-**8**, complex with regard to the corre-

(80) Toth, A.; Floriani, C.; Chiesi-Villa, A.; Guastini, C. *Inorg. Chem.* **1987**, *26*, 236−241.
(81) Reedy, R. J.; Murthy, N. N.; Karlin, K. D.; Blackburn, N. J. *J. Am. Chem. Soc.* **1995**, *117*, 9826−9831.
(82) Rasika Dias, H. V.; Lu, H.-L.; Gorden, J. D.; Jin, W. *Inorg. Chem.* **1996**, *35*, 2149−2151.
(83) Rawlings, J.; Hengge, A. C.; Cleland, W. W. *J. Am. Chem. Soc.* **1997**, *119*, 531−541.
(84) Ardizzoia, G. A.; La Monica, G.; Maspero, A.; Maciocchi, N.; Moret, M. *Eur. J. Inorg. Chem.* **1999**, 1301−1307.
(85) Crabtee, R. H. *The Organometallic Chemistry of the Transition Metals*; Wiley-Interscience: New York, 1994.
(86) (a) Johnson, B. G.; Gill, P. M. W.; Pople, J. A. *J. Chem. Phys.* **1993**, *58*, 5612−5626. (b) Aarnts, M. P.; Stufkens, D. J.; Solà, M.; Baerends, E. J. *Organometallics* **1997**, *16*, 2254−2262.

sponding anti complex, we also find that the CO bond dissociation energy (the negative of the coordination energy in Table 3) for the latter is 8.0 kcal mol^{-1} larger than for the former since it is favored by both terms, the deformation and the interaction energies.

The geometries of the *syn*- and *anti*-$[Cu_2(Me2m)(CO)_2]^{2+}$, **9**, complexes were optimized starting from the already optimized *syn*-$[Cu_2(Me2p)(CO)_2]^{2+}$, *syn*-**8**, complex by merely moving the link of the two methylene groups to the aromatic rings from para to meta locations. For these species, we also find that the syn is more stable than the anti by 5.4 kcal mol^{-1}. The dissociation energy of the CO molecule is now 4.0 kcal mol^{-1} larger for the syn isomer. As compared to the $[Cu_2(Me2p)(CO)_2]^{2+}$, **8**, species (see Table 3), the bond dissociation energy of CO in the *syn*-$[Cu_2(Me2m)(CO)_2]^{2+}$, *syn*-**9**, complex is lower by 3.3 kcal mol^{-1} due to a larger deformation energy (2.0 kcal mol^{-1}) and a slightly less favorable interaction (1.3 kcal mol^{-1}). Finally, the CO dissociation energies of the anti isomers in the $[Cu_2(Me2p)(CO)_2]^{2+}$, **8**, and $[Cu_2(Me2m)(CO)_2]^{2+}$, **9**, complexes are quite similar, the latter being larger by only 0.7 kcal mol^{-1}.

The optimization of the *anti*-$[Cu_2(Me3p)(CO)_2]^{2+}$ complex was started from the X-ray structure of the analogous *anti*-$[Zn_2(Me3p)(NO_3)_2]^{2+}$ complex.[87] The syn complex was optimized from the anti optimized form, by taking one of the two QM fragments and turning it upside down. In comparison with a strict tetrahedral coordination, the locations of the nitrogen atoms around the copper atom in the $[Cu_2(Me3p)(CO)_2]^{2+}$ complexes are less distorted than those of the *anti*-$[Cu_2(Me2p)(CO)_2]^{2+}$, *anti*-**8**, species (compare for instance the NCuN angles Table 2) due to the higher flexibility of the propylenic ligands.

For these species, we find low bond dissociation energies of CO and a similar stability of the syn and anti forms, the anti being somewhat more stable.

For the $[Cu_2(Me3m)(CO)_2]^{2+}$ complexes, we started the optimization from the geometry of the previously optimized *anti*-$[Cu_2(Me3p)(CO)_2]^{2+}$ complexes by just changing the link of two xylylic groups from para to meta locations. Similar energetic results as in the previous case are found here.

NMR Spectroscopy and Fluxional Behavior. The ^{1}H NMR spectra at 320 K of the d^{10} copper(I) complexes described in the present work are characterized by broad nonresolved signals due to the presence of fluxional behavior between different conformational isomers. A detailed analysis of this phenomenon was undertaken using complex $[Cu_2(Me2p)(t\text{-BuNC})_2](ClO_4)_2$, **10**. The ^{1}H NMR spectra of complex **10** recorded in acetone-d_6 at different temperatures are presented in Figure 2. NOESY spectra at 250, 270, and 300 K for complex **10** are presented as Supporting Information. Similar spectra for compound $[Cu_2(Me2m)(t\text{-BuNC})_2](CF_3SO_3)_2$, **11**, are also collected as Supporting Information.

At 320 K, the aromatic region contains two broad singlets at 7.67 and 7.03 ppm. Upon lowering the temperature, the second signal broadens, and finally, at 220 K, it splits into two new signals centered at $\delta = 7.25$ and 6.62 ppm. Further lowering of the temperature to 190 K results in the decoalescence of the initial 7.67 ppm signal into two new singlets centered at 7.59 and 7.75 ppm. The evolution of the aliphatic region of the spectra in the same range of temperatures is rather complex, and a full understanding requires the use of bidimensional experiments. In general, though, lowering of the temperature changes the initially broad features into well-resolved signals. Analysis of the spectra reveals that the complex contains a plane of symmetry, crossing perpendicularly to the two aromatic rings, that divides the macrocycle in two parts magnetically and chemically equivalent. In addition, each of the CH_2 groups of the molecule is a geminal diastereotopic system. Finally, the presence of four different aromatic protons is evident. Further analysis was performed on the basis of NOESY spectra at different temperatures (Supporting Information). The proposed structure of the complex on the basis of these spectra is showed in Scheme 2.

Assignment is based on the observation in the spectra at 250 K of NOEs from H_5 with H_3 and H_7, H_6 with H_4 and H_8, H_{11} with H_{13} and H_{10}, and finally, H_{12} with H_{14} and H_9. NOEs between H_1/H_2 and H_3/H_4 and also between H_{15}/H_{16} and H_{13}/H_{14} allow for the assignment of the aromatic protons. The relative orientation of the methyl groups is also inferred from this experiment; Me_{19} experiences NOEs with H_7 and H_9, Me_{17} with H_{14} and H_{12}, and finally, Me_{18} with H_4, H_{13}, and H_{11}. Aromatic protons H_1 and H_2, equivalent at this temperature, are assigned according to the observation of an NOE with H_3, and H_4. Similarly, H_{15} and H_{16}, also equivalent at this temperature, can be assigned on the basis of NOEs with H_{13} and H_{14}.

The X-ray structure of $[Cu_2(Me2p)(CO)_2](ClO_4)_2$, **8**, indicates that the two aromatic rings are oriented almost perpendicularly relative to each other leading to four different aromatic protons, which are perfectly resolved in the ^{1}H NMR spectra of $[Cu_2(Me2p)(t\text{-BuNC})_2](ClO_4)_2$, **10**, at 190 K. Two aromatic protons, H_{16}, are oriented toward the second aromatic ring, while H_{15} protons are oriented in the opposite direction. H_1 and H_2 point perpendicularly to the plane defined by H_{15} and H_{16}, upward and downward of the macrocyclic plane. Discrimination between H_{15} and H_{16} relies on the basis that the protons oriented toward the aromatic ring should be significantly upshifted.

Variable temperature NOESY experiments also allow the study of the dynamic properties of the molecule. At 270 K, chemical interchange between H_3 and H_{14}, H_4 and H_{13}, H_5 and H_{12}, H_6 and H_{11}, Me_{17} and Me_{18}, as well as among the aromatic protons, is observed. This suggests that the Cu−N bonds next to the benzylic CH_2 (Me_{18} and Me_{17}) are weak, such that they can break allowing the exchange between the two aliphatic chains. H_7, H_8, H_9, and H_{10} remain unaltered in this process. Schematic representation of the different isomeric forms involved in these equilibria is shown in Scheme 3.

The spectra are consistent with the presence of four different interconverting isomers, A, C, E, and G, each of

(87) Anda, C.; Llobet, A. Unpublished results.

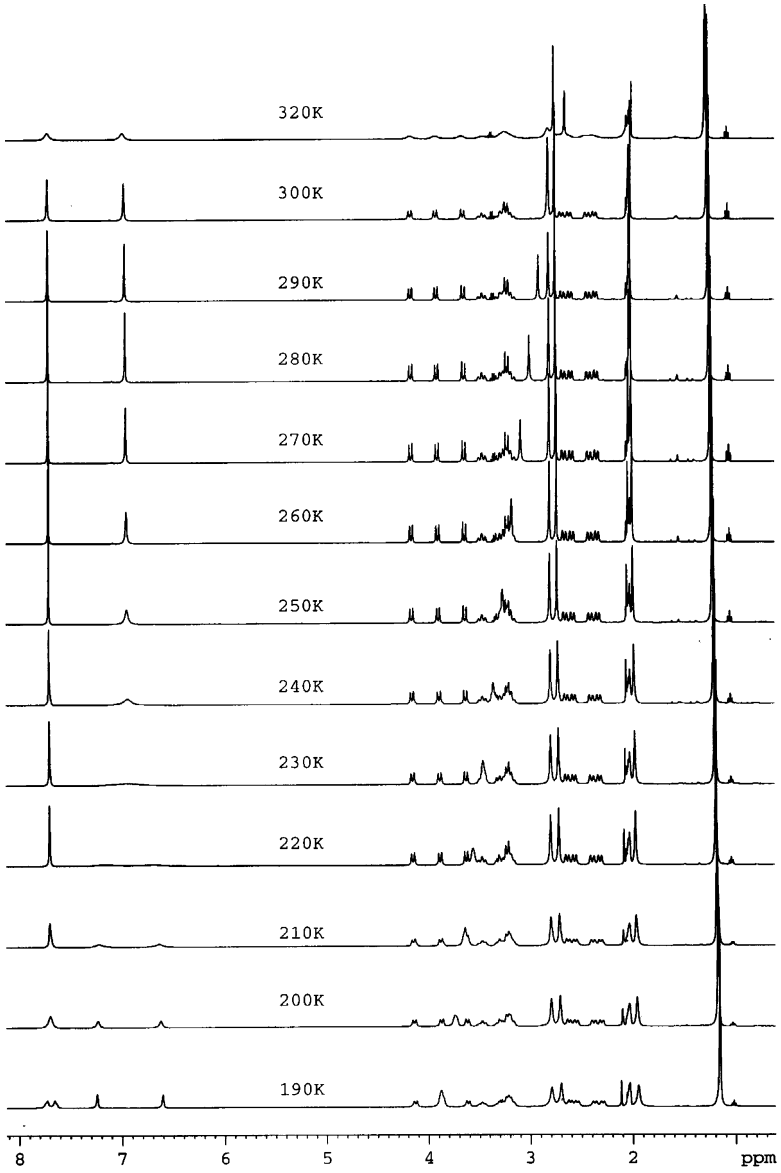

Figure 2. VT ^{1}H NMR spectra of $[Cu_2(Me2p)(t\text{-BuNC})_2](ClO_4)_2$, **10**, in acetone-$d_6$.

Scheme 2. Partial Structural Drawing of Complex $[Cu_2(Me2p)(t\text{-BuNC})_2](ClO_4)_2$, **10**, in Solution at Low *T* with the Corresponding ^{1}H NMR Assignment (ppm)[a]

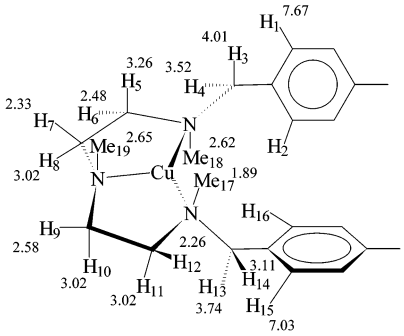

[a] The isocyanide *t*-BuNC ligand is not shown for clarity reasons.

which contains a plane of symmetry. Isomeric forms A and G are predominant at this temperature. Inversion of Me_{17} or Me_{18} results in nonsymmetric forms B, D, H, and F, which undergo a second Me_{17} or Me_{18} inversion faster than the ^{1}H NMR time scale.

At 300 K (Figure S3), interchange phenomena are extended to the four benzylic protons (H_3, H_4, H_{13}, and H_{14}) and also among H_5, H_6, H_{11}, and H_{12}. H_7, H_8, H_9, and H_{10} also interchange at this temperature, indicating that the third Cu−N bond (Cu−NMe_{19}) is also breaking and forming continuously. From this temperature, thermal energy accelerates interchange processes, and at 323 K, H_1−H_2 and H_{15}−H_{16} collapse into an aromatic singlet, H_3, H_4, H_{13}, and H_{14} collapse into a benzylic singlet, the corresponding signals to Me_{17} and Me_{18} also become a singlet, and H_5−H_{12} appear together as a broad singlet. Additional increase of the temperature results in the sharpening of the signals suggesting that the interchange processes become faster than the ^{1}H NMR time scale. The study of the conditions of coalescence of H_{15} and H_{16} reveals that the activation energy for interconversion between both protons is 10.10 kcal/mol.[88] Similarly, interconversion between H_1 and H_2 has an activation barrier of 9.34 kcal/mol. Finally, the barrier for the interconversion between the two aromatic rings is 14.92 kcal/mol.

Scheme 3. Different Isomeric Forms of Compound $[Cu_2(Me2p)(t\text{-BuNC})_2](ClO_4)_2$, **10**, at 270 K

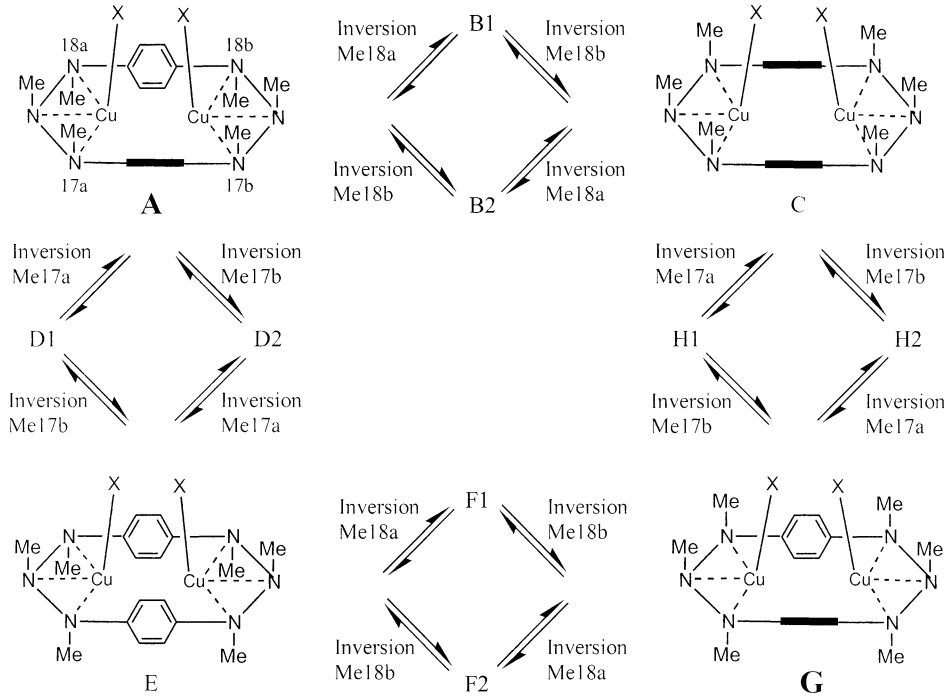

Discussion

Para versus Meta Substitution Effect in the Macrocyclic Ligands. The simple change in the aromatic substitution of the macrocyclic ligands from para to meta produces a shrinkage of cavity by two member ring units. While the local geometry of the copper complexes remains relatively unaffected by this modification, the relative geometry between the two copper centers changes dramatically, even though the Cu···Cu metal distance is not significantly different (6.810 Å for $[Cu_2(Me2p)(CO)_2]^{2+}$, **8**; 6.860 Å for DFT calculated $[Cu_2(Me2m)(CO)_2]^{2+}$, **9**; 6.776 Å for $[Cu_2(Me2m)(t\text{-BuNC})_2]^{2+}$, **11**). A feature that illustrates this difference is the relative orientation of the terminal ligands bonded to the copper metal center. For the $[Cu_2(Me2p)(CO)_2]^{2+}$, **8**, complex, the vectors defined by the terminal CO ligand face each other with a torsion angle of only 5.6°. In the case of $[Cu_2(Me2m)(L)_2]^{2+}$, the vectors defined by the NC bond (L = *t*-BuNC, **11**) of the isocyanide ligand and by the CO bond (L = CO, **9**) are tilted by 76.5° and 80.0°, respectively. In order to further compare the relative geometrical rearrangement between the copper metals, it is interesting to point out here the distances between these terminal ligands. Thus, the O5···O55 distance for the $[Cu_2(Me2p)(CO)_2]^{2+}$, **8**, complex is only 3.122 Å while the equivalent distance for $[Cu_2(Me2m)(CO)_2]^{2+}$, **9**, is 4.063 Å, and for $[Cu_2(Me2m)(t\text{-BuNC})_2]^{2+}$, **11**, the equivalent N···N distance is 3.989 Å.

Syn versus Anti Preferences. X-ray diffraction analysis and low *T* NMR are consistent with the presence of the same single isomer in the solid-state and in solution. For complexes $[Cu_2(Me2p)(CO)_2]^{2+}$, **8**, and $[Cu_2(Me2m)(CO)_2]^{2+}$, **9**, this single isomer has a syn conformation with regard to the relative orientation of the terminal carbonyl ligands (see Figure 1A).

At first glance, one would expect the anti conformation for complex $[Cu_2(Me2p)(CO)_2]^{2+}$, **8**, to be more energetically stable than the syn given the steric hindrance caused by the proximity of the carbonyl ligands facing each other. In order to understand the origin of this unexpected phenomenon, a theoretical study was undertaken using the ADF type of calculations for dicarbonyl dinuclear copper complexes containing the four ligands studied in the present work both in the syn and anti conformations. We have found that the larger bond dissociation energy of CO in the syn species is due in part to a smaller deformation energy of the $[Cu_2(Me2p)(CO)]^{+2}$, **8**, fragment (without a CO molecule) and also to a more favorable interaction energy in the syn form. This is also reflected in the larger C−O bond length in the syn complex as compared to the anti.

The key interactions between the incoming CO molecule and the $[Cu_2(Me2p)(CO)]^{2+}$ fragment (without one CO ligand) involve, first, the donation from the HOMO σ-orbital of CO, which corresponds to the lone pair on the C atom, to the unoccupied 1b orbital ($2a_1$* in C_{3v} symmetry; see Scheme 4[89]) of the $[Cu_2(Me2p)]^{2+}$ fragment, and second, the back-donation from the occupied 1a orbital ($1e_a$ in C_{3v} symmetry) of the metal complex fragment to the LUMO π*-orbital of CO. One can therefore understand the particular position of the two CO molecules one facing the other since back-donation is specially favored when the CO molecule is

(88) $\Delta G^{\ddagger} = RT_c[22.96 + \ln(T_c/\Delta\delta)]$, where T_c is coalescence temperature and $\Delta\delta$ is the difference in the ^{1}H NMR shift of the two decoalescenced signals at T_c. See for example: Ritzeler, O.; Parel, S.; Therrien, B.; Bensel, N.; Reymond, J.-L.; Schenk, K. *Eur. J. Org. Chem.* **2000**, 1365−1372.

(89) Albright, T. A.; Burdett, J. K.; Whangbo. M−H. *Orbital Interactions in Chemistry*; Wiley-Interscience: New York, 1985; p 383.

Scheme 4. Drawing of HOMO (1a) and LUMO (1b) Molecular Orbitals for a ML_3 Fragment with C_{3v} Symmetry

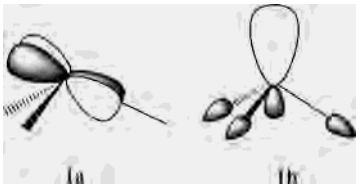

somewhat tilted. In such a position, the overlap between the LUMO π*-orbital of CO and the 1a orbital is maximized.

As a whole, the preference of the CO ligand to coordinate in the syn form in both the Me2p and Me2m can be attributed to more favorable orbital interaction energy and reduced strain energy of the ligand in this isomer.

In sharp contrast for the Me3p and Me3m complexes, the energy strain of the ligands is reversed with the syn isomers being more difficult to deform than the anti ones. The interaction energies are similar in both isomers, and this is also reflected in their almost identical C−O bond lengths. On balance, the two isomers end up with very similar energies but slightly favor the anti.

Steric and Electronic Factors Influencing the Coordination Number and Geometry of Copper(I) Complexes. The complexes $[Cu_2(Me2p)L_2]^{2+}$ and $[Cu_2(Me2m)L_2]^{2+}$ display a rather distorted tetrahedral arrangement around the metal center as shown in the Results section. This distortion is imposed by the rigidity of the macrocyclic ligand forming a five-member chelate ring and because of the lack of crystal field stabilization energy for a d^{10} ion. Thus, NCuN bond angles of 85.6° are obtained which are rather far from the ideal 109.47°.

The stability of this family of copper(I) complexes with regard to oxidative processes follows the order L = CH_3CN < CO < PPh_3 < *t*-BuNC. This reflects the strength of the Cu(I)−L bond and the capacity of good σ-donor/π-acceptor ligands to stabilize low oxidation states.

For the present carbonyl and isocyanide complexes, IR spectroscopy unambiguously indicates a terminal coordination mode of the monodentate ligand. Furthermore, the presence of a single band in both cases also indicates that both copper centers are symmetrically related even though this symmetry does not strictly exist in the respective X-ray structures at low temperatures. IR spectroscopy is also very useful to put forward and monitor the existence of a substitution reversible process as shown in eq 3, which is also indicative of the lability of the Cu−C bond. The lability of the rest of the metal−ligand bonds (Cu−N bonds) is also evidenced by variable *T* NMR spectroscopy.

$[Cu_2(Me3p)]^{2+}$ (**4** and **5**) and $[Cu_2(Me3m)]^{2+}$ (**6** and **7**) are isolated as tricoordinated complexes in the solid-state. IR spectroscopy is again a very useful tool that allows us to monitor the reaction of these complexes with carbon monoxide in acetone to form presumably the corresponding tetracoordinated complexes $[Cu_2(L)(CO)_2]^{2+}$ (L = Me3p and Me3m) (ν = 2060 cm^{-1}). It is interesting to note that this reaction does not take place using acetonitrile as the solvent in agreement with the existence of the following equilibrium

$$[Cu_2(Me3p)(MeCN)_2]^{2+} \rightleftarrows [Cu_2(Me3p)]^{2+} + 2\ MeCN \quad (5)$$

which had been previously proposed by Karlin in related complexes.[90,91] The low CO stretching frequency displayed by $[Cu_2(L)(CO)_2]^{2+}$ (L = Me3p and Me3m) resembles those of copper-containing proteins possessing tris(imidazole) coordination cores for the copper center (hemocyanins, amine oxidases, peptidylglycine monooxygenase, and cytochrome C oxidase) which exhibit ν(CO) in the range 2043−2063 cm^{-1}.[92−94] Such a low frequency range in synthetic complexes had only been observed so far with nonchelating imidazole ligands or anionic tris(pyrazolyl)borate ligands. On the other hand, $[Cu_2(L)(CO)_2]^{2+}$ (L = Me2p, **8**, and Me2m, **9**) display a single ν(CO) at 2087 cm^{-1}, which falls in the 2080−2102 cm^{-1} range commonly found for complexes containing neutral ligands.

From a structural viewpoint, the ligands bearing three methylenic units between tertiary amines have a better geometric arrangement than those with two to better fit the demands of a tetrahedral coordination, giving rise to six-member chelate rings with the metal center. Thus, now the lowest NCuN bond angle is 96.08° in contrast with the 85.07° of the previous structurally described complexes.

From an electronic viewpoint, the addition of two methylenic units per copper center produces a significant enhancement of electronic density over the tertiary amine and in turn to the metal center. This is supported experimentally by potentiometric titration studies of the free ligand[87] and theoretically by the values of the Mulliken charge obtained on the ligand (+1.29 and +1.42 electrons for the *syn*-$[Cu_2(Me2p)(CO)_2]^{2+}$, **8**, and *syn*-$[Cu_2(Me3p)(CO)_2]^{2+}$ complexes, respectively).

Furthermore, as a consequence of this greater charge transfer, the energy of the 1b orbital in the $[Cu_2(Me3p)]^{2+}$ fragment is raised by about 0.5 eV. In turn, the donation from the HOMO σ-orbital of CO to the unoccupied 1b orbital is reduced, thus in turn decreasing the back-donation from the 1a orbital to the LUMO π* orbital of CO. This effect is clearly seen in the bond dissociation energies of the CO molecule gathered in Table 3. As compared to the $[Cu_2(Me2p)(CO)_2]^{2+}$, **8**, counterparts, the $[Cu_2(Me3p)(CO)_2]^{2+}$ species have bond dissociation energies of CO that are about 10 kcal mol^{-1} lower, in agreement with the fact that experimentally CO is easily removed from the *anti*-$[Cu_2(Me3p)(CO)_2]^{2+}$ complex.

Overall, the electronic factor just described favors tricoordination over tetracoordination for copper(I) complexes with ligands containing three methylenic units, and thus shifts eq 4 to the left.

(90) Karlin, K. D.; Haka, M. S.; Cruse, R. W.; Meyer, G. J.; Farooz, A.; Gultneh, Y.; Hayes, J. C.; Zubieta, J. *J. Am. Chem. Soc.* **1988**, *110*, 1196−1207.
(91) Karlin, K. D.; Tyeklar, Z.; Farooq, A.; Ghosh P.; Cruse, R. W.; Gultneh, Y.; Hayes, J. C.; Toscano, P. J.; Zubieta, J. *Inorg. Chem.* **1992**, *31*, 1436−1451.
(92) We thank one of the reviewers for making us aware of this similarity.
(93) Rondelez, Y.; Sénèque, O.; Rager, M.-N.; Duprat, A. F.; Reinaud, O. *Chem. Eur. J.* **2000**, *6*, 4218−4226.
(94) Zhang, C. X.; Kaderli, S.; Costas, M.; Kim, E.-i.; Neuhold, Y.-M.; Karlin, K. D.; Zuberbühler, A. D. *Inorg. Chem.* **2003**, *42*, 1807−1824.

Conclusions and Future Perspectives. The four macrocyclic ligands described in the present paper allow us to gain a certain control of the chemical properties of their corresponding copper(I) dinuclear complexes. In particular, it turns out that the number of methylenic units, two or three, bonding each tertiary amine in the ligands, significantly influences (a) the copper(I) tendency to three or four coordination and (b) relative spatial arrangement between copper(I) metal centers (syn vs anti). Preliminary results related to the oxidative chemistry of these complexes reveal that these two parameters, carefully controlled, produce different reactivity patterns. We are at present dedicating our efforts toward the characterization and rationalization of the oxidative reactivity of these complexes both in an stoichiometric and a catalytic manner.

Acknowledgment. This research has been financed by MCYT of Spain through Project BQU2000-0458. A.L. is grateful to CIRIT Generalitat de Catalunya (Spain) for the Distinction Award and the Aid SGR2001-UG-291. M.C. and R.X. are grateful to CIRIT and UdG, respectively, for the allocation of doctoral grants. J.R. acknowledges partial support from CONACYT (Mexico) and from the Visiting Professors Grant (PIV Program, del Comissionat per a Universitats i Recerca del Departament de la Presidència de la Generalitat de Catalunya) to fund a sabbatical visit to the Institut de Química Computacional (IQC) of the University of Girona, Catalonia, Spain, and he is grateful for the great hospitality at IQC. M.S. acknowledges support for this work under Grant PB98-0457-C02-01 and BQU2002-04112-C02-02 from the Dirección General de Enseñanza Superior e Investigación Científica y Técnica (MEC-Spain). He is also indebted to the Departament d'Universitats, Recerca i Societat de la Informació of the Generalitat de Catalunya, for financial support through the Distinguished University Research Promotion, 2001.

Supporting Information Available: Bidimensional NMR spectral characterization data for **10** and **11**, VT NMR spectral characterization data for **11**. Cartesian atomic coordinates for all the calculated complexes. Crystallographic information files (CIFs) for **8** and **11**. This material is available free of charge at http://pubs.acs.org.

IC0261833